Research Article

Detection of Ground Moving Targets for Two-Channel Spaceborne SAR-ATI

Zhen Dong,[1] Bin Cai,[2] and Diannong Liang[1]

[1] *School of Electronic Science and Engineering, National University of Defense Technology (NUDT), Changsha, Hunan, 410073, China*
[2] *Telecommunication Engineering Institute, Air Force Engineering University, Xi'an, Shanxi, 710077, China*

Correspondence should be addressed to Zhen Dong, dongzhen@vip.sina.com

Many present spaceborne synthetic aperture radar (SAR) systems are constrained to only two channels for ground moving target indication (GMTI). Along-track interferometry (ATI) technique is currently exploited to detect slowly moving targets and measure their radial velocity and azimuth real position. In this paper, based on the joint probability density function (PDF) of interferogram's phase and amplitude and the two hypotheses "clutter" and "clutter plus signal", several constant false alarm rate (CFAR) detection criteria are analyzed for their capabilities and limitations under low signal-to-clutter ratio (SCR) and low clutter-to-noise ratio (CNR) conditions. The CFAR detectors include one-step CFAR detector with interferometric phase, two-step CFAR detectors, and two-dimensional (2D) CFAR detector. The likelihood ratio test (LRT) based on the Neyman-Pearson (NP) criterion is exploited as an upper bound for the performance of the other CFAR detectors. Performance analyses demonstrate the superiority of the 2D CFAR techniques to detect dim slowly moving targets for spaceborne system.

1. Introduction

Many present spaceborne synthetic aperture radar (SAR) systems, such as TerraSAR-X and RADARSAT-2, are constrained to two channels to detect slowly moving targets on the ground. The two channels, which aligned in the flight direction of the same or different platform(s), observe the same terrain at different times under identical geometry. The radial velocities of the ground moving targets lead to the phase difference of the two registered SAR images whereas the two channel signals for stationary scene are identical and can be canceled out by computing the phase difference. Along-track interferometry (ATI) technique exploits the interferogram of the two channel SAR images to perform moving target detection, radial velocity measurement, and azimuth relocation.

Traditional SAR-ATI detection techniques only used the interferometric phase as the constant false alarm rate (CFAR) detection metric to separate moving target from clutter. Gierull [1, 2] derived the theoretical joint (PDF) probability density function (PDF) of interferogram's phase and amplitude for the hypotheses "clutter" and "clutter plus signal" under the assumption of Gaussian backscatter. A two-step CFAR detector [1] is also proposed by computing the magnitude and phase thresholds separately based on the marginal PDFs of magnitude and phase. Chiu [3] proposed a nonparametric CFAR detector using histogram approximation to the theoretical joint PDF for the clutter interferogram. Meyer et al. [4] integrated a prior information into a likelihood ratio detector, which include road network database and the radar cross-section (RCS) of the moving targets. This new hypothesis-test framework is fit for public traffic monitoring applications, where the vehicles are assumed to travel strictly on streets or roads.

In fact, two-channel ATI technique is not a clutter-cancellation technique, which only nulls the clutter interferometric phase but does not improve the signal-to-clutter ratio (SCR) as other clutter suppression techniques. For decreasing SCR values, the interferometric phase of the "clutter plus target" migrate from the true target phase value towards zero on one hand, and increase in variance on the other hand. The nonnegligible clutter contamination to target signal may lead to significant decrease of performance for target detection and velocity estimation [5]. Cross-channel decorrelations of

clutter returns, such as channel unbalance or the additive receiver thermal noise, are other limitations to ATI detection performance, but some of them can be remedied using suitable calibration techniques [2, 5]. At low clutter-to-noise ratio (CNR) patches, such as smooth roads or water surfaces, the correlation value may be lower to 0.8. Due to the low coherence, the wide phase distribution of the clutter interferogram induces that the phase detection threshold becomes too large, and prohibits almost any detection [2]. In this paper, under low SCR or low CNR conditions, several CFAR techniques are analyzed for their capabilities and limitations.

In this paper, based on the joint probability density function (PDF) of interferogram's phase and amplitude and the two hypotheses "clutter" and "clutter plus signal", several constant false alarm rate (CFAR) detection criteria are analyzed for their capabilities and limitations under low signal-to-clutter ratio (SCR) and low clutter-to-noise ratio (CNR) conditions. The CFAR detectors include one-step CFAR detector with interferometric phase, two-step CFAR detectors and two-dimensional (2D) CFAR detector. The likelihood ratio test (LRT) based on the Neyman-Pearson (NP) criterion is exploited as an upper bound for the performance of the other CFAR detectors.

The paper is organized as follows. Section 2 reviews the statistics of the multilook interferograms' magnitude and phase for the hypotheses "clutter" and "clutter plus moving target" under Gaussian assumption of the clutter. Section 3 describes the CFAR detection techniques and the likelihood ratio test (LRT) under the NP (Neyman-Pearson) criterion. Performance analysis and comparison are given in Section 4. Section 5 gives the conclusion.

2. Statistics of Multilook Interferograms' Magnitude and Phase for the Hypotheses "Clutter" and "Clutter Plus Moving Target"

Firstly, some realistic assumptions are described as follows: (i) Gaussian distributed stationary clutter which is validated over homogeneous agricultural and natural areas [1]; (ii) moving target is modeled as point target of Swerling 0 case with a constant velocity; (iii) magnitude and phase errors caused by mismatched SAR processing or channel unbalance have been eliminated prior to the detection; (iv) the SAR resolution cell is larger than the target size that contains both clutter and moving target; (v) the definitions of SCR and CNR are proposed in [6], which are different from traditional definitions used in GMTI. Under above assumptions, the well-known joint PDF of the multilook interferograms' phase Φ and normalized magnitude η for the clutter-only case is given by [1]

$$
f_c(\eta, \Phi) = \frac{2n^{n+1}\eta^n}{\pi\Gamma(n)(1-\rho^2)} \cdot \exp\left(\frac{2n\eta\rho\cos\Phi}{1-\rho^2}\right)
$$
$$
\times K_{n-1}\left(\frac{2n\eta}{1-\rho^2}\right), \quad -\pi < \Phi \leq \pi, \ \eta \geq 0, \tag{1}
$$

where ρ is the correlation coefficient between the two channel outputs and n is the effective number of looks. $K_{n-1}(\cdot)$ is the
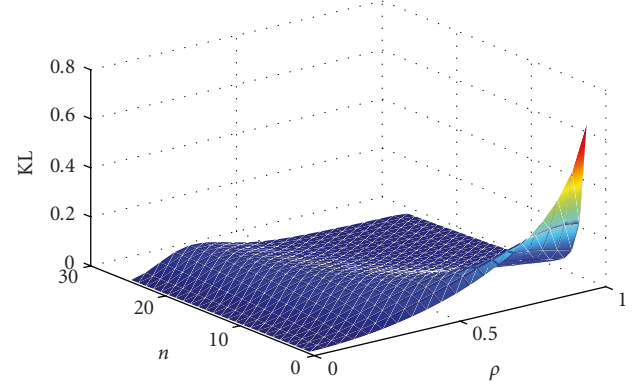

FIGURE 1: Kullback-Leibler (KL) divergence of joint PDF and product of the marginal PDF for different looks number and the coherence.

second type modified Bessel function of order $(n - 1)$, and $\Gamma(\cdot)$ is the gamma function. Integrating (1) with respect to η or Φ lead to the marginal PDFs of the phase and magnitude as follows:

$$
f_c(\Phi) = \frac{\Gamma(n + 1/2)(1 - \rho^2)^n\rho\cos(\Phi)}{2\sqrt{\pi}\Gamma(n)(1 - \rho^2\cos^2(\Phi))^{(n+1/2)}}
$$
$$
+ \frac{(1 - \rho^2)^n}{2\pi}\ {}_2F_1\left(n, 1; \frac{1}{2}; \rho^2\cos^2(\Phi)\right), \tag{2}
$$

$$
f_c(\eta) = \frac{4n^{n+1}\eta^n}{\Gamma(n)(1 - \rho^2)}I_0\left(\frac{2n\eta\rho}{1 - \rho^2}\right) \cdot K_{n-1}\left(\frac{2n\eta}{1 - \rho^2}\right),
$$

where ${}_2F_1(\cdot)$ is the Gauss's hypergeometric function, and $I_0(\cdot)$ is the first type modified Bessel function of zero. Kullback-Leibler (KL) divergence can be used to show the degree of the dependence between magnitude and phase, which is defined as

$$
\mathrm{KL}(f_c(\eta, \Phi), f_c(\eta) \cdot f_c(\Phi))
$$
$$
= \int_{-\pi}^{\pi}\int_0^{+\infty} f_c(\eta, \Phi)\log\left[\frac{f_c(\eta, \Phi)}{f_c(\eta) \cdot f_c(\Phi)}\right]d\eta d\Phi. \tag{3}
$$

Because the PDF of (1) and (2) depend only on the number of looks and the coherence, the KL divergence are plotted in Figure 1 as a function of the two parameters using numerical integration. For $0 < \rho \leq 1$ and $0 < n \leq 25$ in the figure, it is clear that η and Φ are not statistically independent, where the KL divergence become large as the coherence increase and the looks number decrease. As the KL divergence of (3) shown in Figure 1, the interferometric magnitude and phase cannot be assumed to be independent for most cases.

For large number of looks, the approximation PDF of "clutter plus moving target" is given as [2]

$$
\begin{aligned}
&f_{c+m}(\eta, \Phi) \\
&= \frac{2n^{n+1}\eta\left(\left(\eta - \delta\cos(\Phi - \Phi_v)\right)^2 + \delta^2\sin^2(\Phi - \Phi_v)\right)^{(n-1)/2}}{\pi\Gamma(n)(1 - \rho^2)} \\
&\quad \cdot \exp\left(\frac{2n\rho(\eta\cos(\Phi) - \delta\cos(\Phi_v))}{1 - \rho^2}\right) \\
&\quad \cdot K_{n-1}\left(\frac{2n\sqrt{(\eta - \delta\cos(\Phi - \Phi_v))^2 + \delta^2\sin^2(\Phi - \Phi_v)}}{1 - \rho^2}\right),
\end{aligned}
\tag{4}
$$

where Φ_v is the interferometric phase of moving target and δ is the signal-to-clutter ratio (SCR). n, ρ are defined in (1). The analytical integration of (4) with respect to the magnitude or phase to get the marginal PDF is extremely difficult or even impossible. Alternatively, numerical integration can be used to calculate the theoretical PDF of phase or magnitude.

3. CFAR Detectors and Likelihood Ratio Test Based on the Optimum NP Criterion

3.1. One-Step CFAR Detector with Interferometric Phase. The common used CFAR test statistic for ATI is the interferometric phase, which is robust for scene heterogeneity and channel power unbalance. The test cell's interferometric phase is compared with a chosen threshold. For given probability of false alarm ($P_{fa} = \alpha$), the phase threshold $|\Phi_{th}|$ can be determined using (5) and the probability of detection (P_d) can be computed using (6). The involved parameters, such as the number of looks and the coherence, are estimated directly from the two-channel SAR data [1]:

$$
P_{fa} = 2\int_{|\Phi_{th}|}^{\pi} f_c(\Phi)d\Phi = \alpha,
\tag{5}
$$

$$
P_d = 2\int_{|\Phi_{th}|}^{\pi} f_{c+m}(\Phi)d\Phi.
\tag{6}
$$

As several papers have analyzed [1, 2, 4], the multilook number should be chosen $n \geq 4$ to get reasonable P_{fa} ($P_{fa} \leq 10^{-5}$) for the phase-only CFAR detection. In this paper, we choose $n = 10$. Typical SAR signal decorrelations in the technique include image misregistration, channel unbalance, Doppler discrepancy, temporal scene decorrelation, quantization error, uncorrelated SAR impulse response tails, and the thermal noise. For simplification, other coherence except for the thermal noise coherence are chosen to be one. Assume the two SAR signals have the same CNR, the correlation coefficient can be expressed as

$$
\rho = \frac{\text{CNR}}{\text{CNR} + 1}.
\tag{7}
$$

The PDFs of the interferometric phase for the two hypotheses with Φ for $\Phi_v = 1$ rad, $n = 10$, and $P_{fa} = 10^{-5}$ are shown in

Figures 2(a) (CNR = 10 dB, SCR = 10, 5, 0, −5, −∞ dB) and 2(b) (SCR = 0 dB, CNR = 20, 10, 0, −3 dB). When the SCR decrease, the phase PDF of second hypothesis may migrate from Φ_v to zero phase line with variance increase, which are shown in Figure 2(a). When the CNR decreases, the wide phase distribution of the clutter interferogram induces that the phase detection threshold becomes too large, and prohibits almost any detection.

Figure 3 shows the P_d versus SCR or CNR curves with $n = 10$, $P_{fa} = 10^{-5}$, $\Phi_v = 1$ rad, 1.5 rad, 2 rad, 2.5 rad. CNR = 10 dB in Figure 3(a) and SCR = 5 dB in Figure 3(b). From Figure 3, we can see that the phase-only metric loses its ability to detect slowly moving targets and to correctly estimate their velocities under low SCR or CNR conditions. For fast moving targets, due to the SAR focusing technique, the magnitude response of fast moving targets may degrade 50% or more lower. The peak power of the moving target may be comparable to the clutter power. Low SCR and low CNR (or low correlation) may be the major obstacle to the phase-only detector.

3.2. Two-Step CFAR Detectors. Gierull proposed a two-step CFAR detector by computing the magnitude and phase thresholds separately from their marginal PDFs [1]. The first test static is phase and the second test for the remaining pixels is the magnitude. The test cell can be termed to "clutter plus target" hypothesis if its phase and magnitude all exceed the thresholds. The detector is based on the assumptions that clutter with large phase values most likely have a small magnitude and most moving targets have a relatively high RCS [1], which are shown in Figure 4. According to Figure 4, the assumption that moving targets will have a higher RCS than the terrain is fit for most homogeneous clutter regions, except for the urban areas or sea surfaces.

The clutter pixels in the low CNR regions, such as those corresponding to road and water surfaces, can be suppressed by the amplitude marginal detection, but it cannot separate the moving targets from the stationary scene. Therefore, the two detection metrics can be combined to a two-step CFAR detector. For a fixed $P_{fa} = \alpha$, the thresholds η_{th}, $|\Phi_{th}|$ and P_d for the two-step CFAR detector can be determined as

$$
\begin{aligned}
P_{fa} &= 2\int_{\eta_{th}}^{\infty} f_c(\eta)d\eta \cdot \int_{|\Phi_{th}|}^{\pi} f_c(\Phi)d\Phi = \alpha, \\
P_d &= 2\int_{\eta_{th}}^{\infty} f_{c+m}(\eta)d\eta \cdot \int_{|\Phi_{th}|}^{\pi} f_{c+m}(\Phi)d\Phi.
\end{aligned}
\tag{8}
$$

As seen in Figure 1, η and Φ are not statistically independent. The conditional PDF of interferometric magnitude for a fixed phase and the marginal PDF of phase can be used alternatively to improve the detector performance. For a fixed P_{fa}, the thresholds and P_d can be determined by replacing the marginal PDF of magnitude with the conditional PDF in (8):

$$
\begin{aligned}
P_{fa} &= 2\int_{|\Phi_{th}|}^{\pi} f_c(\Phi)d\Phi \cdot \int_{\eta_{th}}^{\infty} f_c(\eta \mid \Phi_{th})d\eta = \alpha, \\
P_d &= 2\int_{|\Phi_{th}|}^{\pi} f_{c+m}(\Phi)d\Phi \cdot \int_{\eta_{th}}^{\infty} f_{c+m}(\eta \mid \Phi_{th})d\eta.
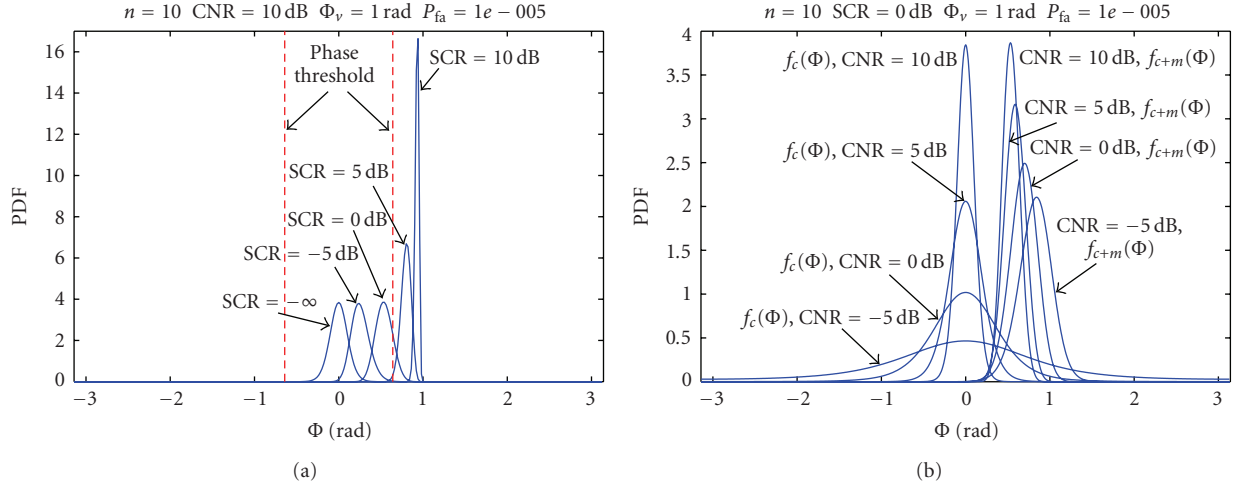\end{aligned}
\tag{9}
$$

FIGURE 2: PDF of the interferometric phase of "clutter" and "clutter plus moving target" with Φ for $n = 10$, $P_{\text{fa}} = 1e - 5$, and $\Phi v = 1$ rad. (a) CNR = 10 dB, SCR = $-\infty$, -5 dB, 0 dB, 5 dB, 10 dB; (b) SCR = 0 dB, CNR = -5 dB, 0 dB, 5 dB, 10 dB for $f_c(\Phi)$ and $f_{c+m}(\Phi)$.
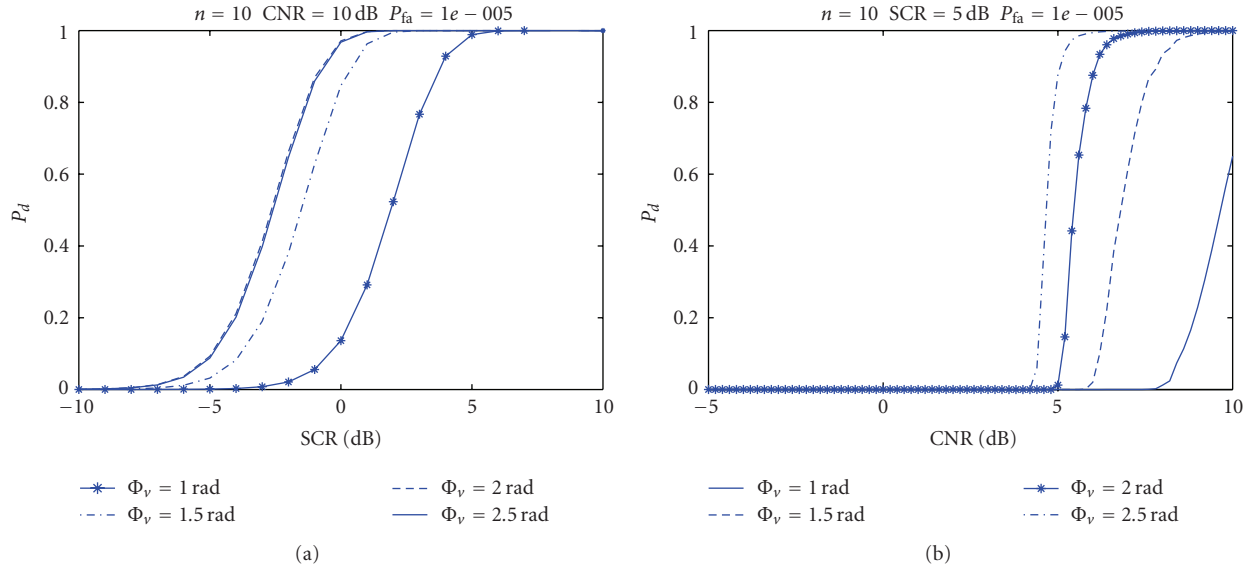

FIGURE 3: P_d versus SCR and CNR of one-step CFAR detector with Φ for $n = 10$, $P_{\text{fa}} = 1e - 5$, $\Phi v = 1$ rad, 1.5 rad, 2 rad, 2.5 rad. (a) CNR = 10 dB; (b) SCR = 0 dB.

Figure 5(a) shows the CFAR thresholds for one-step detection with η, Φ and the threshold curves for two-step detection with marginal PDFs and the conditional PDF for $n = 10$, CNR = 10 dB, SCR = 0 dB, $\Phi_v = 1$ rad, and $P_{\text{fa}} = 10^{-5}$. The joint PDFs of the two hypotheses are also plotted for ease of comparison. Figure 5(b) shows $f_c(\eta \mid \Phi_{\text{th}})$ and the corresponding thresholds (dash lines) changed with Φ_{th} for $n = 10$, CNR = 10 dB, $P_{\text{fa}} = 10^{-3}$. In Figure 5(a), for $P_{\text{fa}} = 10^{-5}$, the P_ds for one-step detection with η or Φ are very low. The conditional PDF of magnitude is much fit to separate moving target from clutter than the marginal PDF. Because η, Φ cannot be assumed independent, Figure 5(b) shows that the PDF of magnitude η is a function of phase. The fluctuations of η distribution become larger as Φ approximate to zero and the CFAR thresholds become larger (dashed lines).

Observe from (8) that the two kinds of two-step CFAR detectors have P_d and P_{fa} that are both dependent on two thresholds. Under a fixed P_{fa}, there exist an infinite number of threshold pairs achieving a fixed P_{fa}. The user is left with the task of choosing a threshold pair to operate the detector, that is, an operating point. The choice of an operating point is pivotal to resulting performance and must be chosen carefully. In Figures 6(a) and 6(b), the P_d curves that change along the iso-P_{fa} curves are plotted with 3-D visualization for $P_{\text{fa}} = 10^{-4}$, 10^{-5}, 10^{-6}. To be noted, the threshold pair that maximizes the two-step CFAR detectors' P_d for a fixed P_{fa} is a function of SCR, CNR, n, Φ_v. Since the moving target parameters may not be known, the optimization of P_d is a difficult task. On the other hand, the two-step detector is not CFAR, if the chosen threshold pair for a fixed P_{fa} depends on the signal parameters. As seen from Figure 6, a reasonable
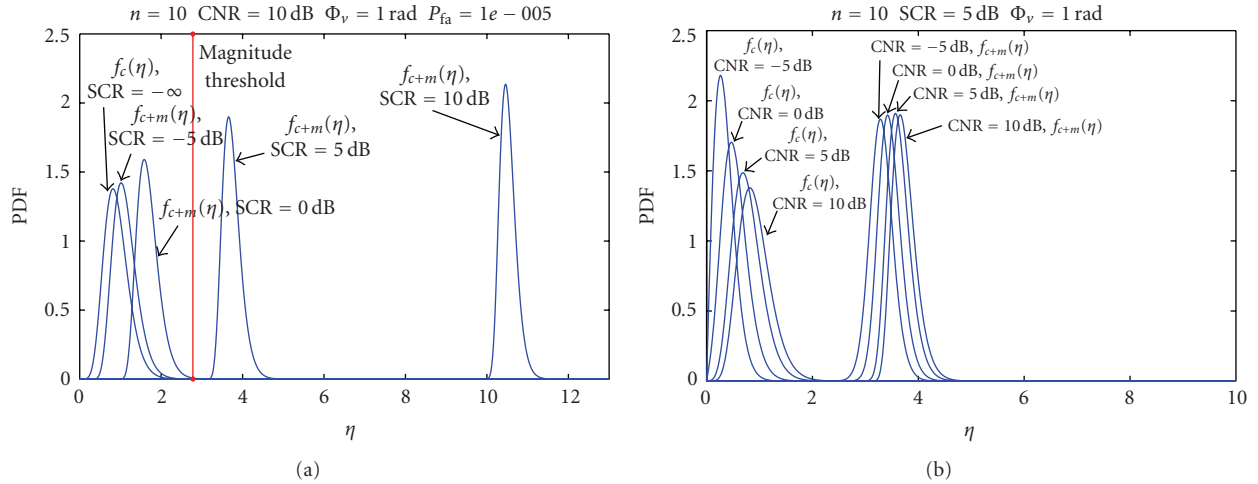
FIGURE 4: PDF of the interferometric magnitude of "clutter"and "clutter plus moving target" with η for $n = 10$, $P_{fa} = 1e-5$, and $\Phi_v = 1$ rad. (a) CNR = 10 dB, SCR = $-\infty$, -5 dB, 0 dB, 5 dB, 10 dB; (b) SCR = 5 dB, CNR = -5 dB, 0 dB, 5 dB, 10 dB for $f_c(\eta)$ and $f_{c+m}(\eta)$.
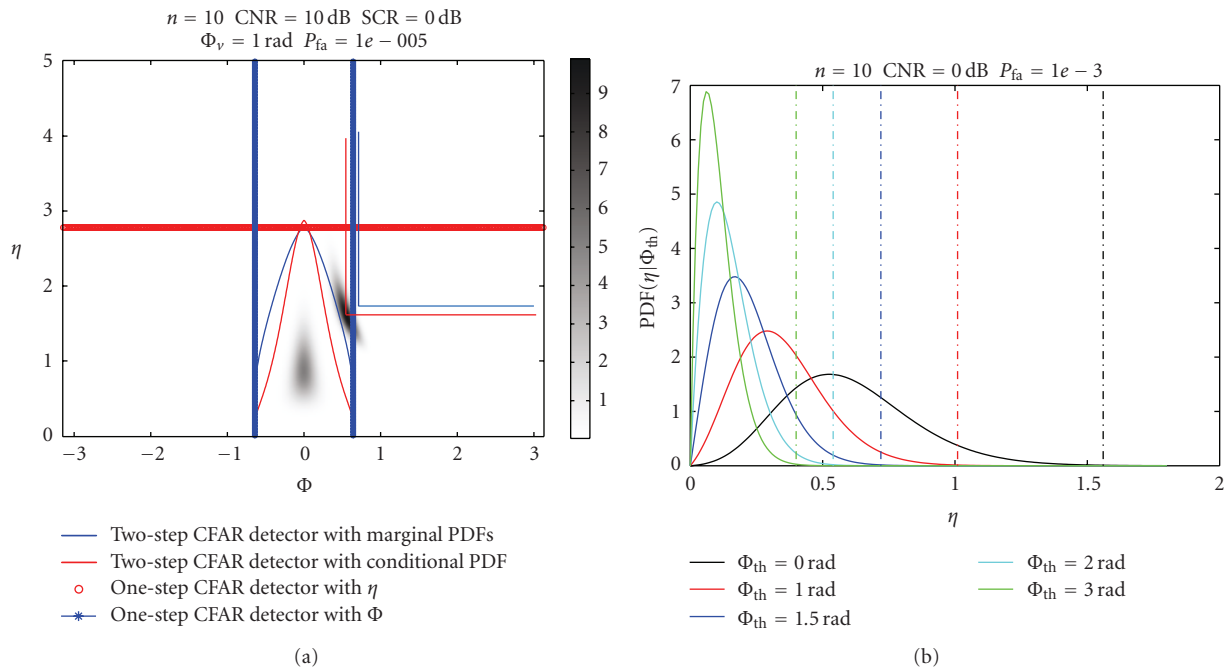

FIGURE 5: (a) Threshold curves of ATI detectors for $n = 10$, $P_{fa} = 1e-5$, CNR = 10 dB, SCR = 0 dB, and $\Phi_v = 1$ rad, (one-step CFAR detector with Φ and η, two-step CFAR detector with conditional PDF, and two-step CFAR detector with marginal PDFs); (b) the PDF of η as a function of phase and corresponding thresholds.

strategy for operating point selection is to choose a point near the center of the iso-P_{fa} curves. At other times, the pairs of thresholds can also be chosen to an interval of points along the iso-P_{fa} curves. In fact, the appropriate operating points along the contours used for detection ultimately depend on system needs [1].

3.3. Two-Dimensional (2D) CFAR Detector. As described in Section 3.2, on one hand, the task of choosing an operating point is very difficult. On the other hand, if one uses a constant magnitude-phase threshold pair arbitrarily, the

result would lead to either too many false alarms or too few detected targets, whether or not takes into account the magnitude dependence of the phase PDF. Based on the theoretical joint PDF of magnitude and phase, it is possible to use false alarm isolines to separate moving targets from clutter on the two-dimensional magnitude-phase plane. However, there exist an infinite number of iso-P_{fa} lines on the plane under different criteria or on the different integral areas. Since the PDF of the "clutter plus moving target" is not known, it is assumed to be uniformly distributed in the entire region. Then, the likelihood ratio
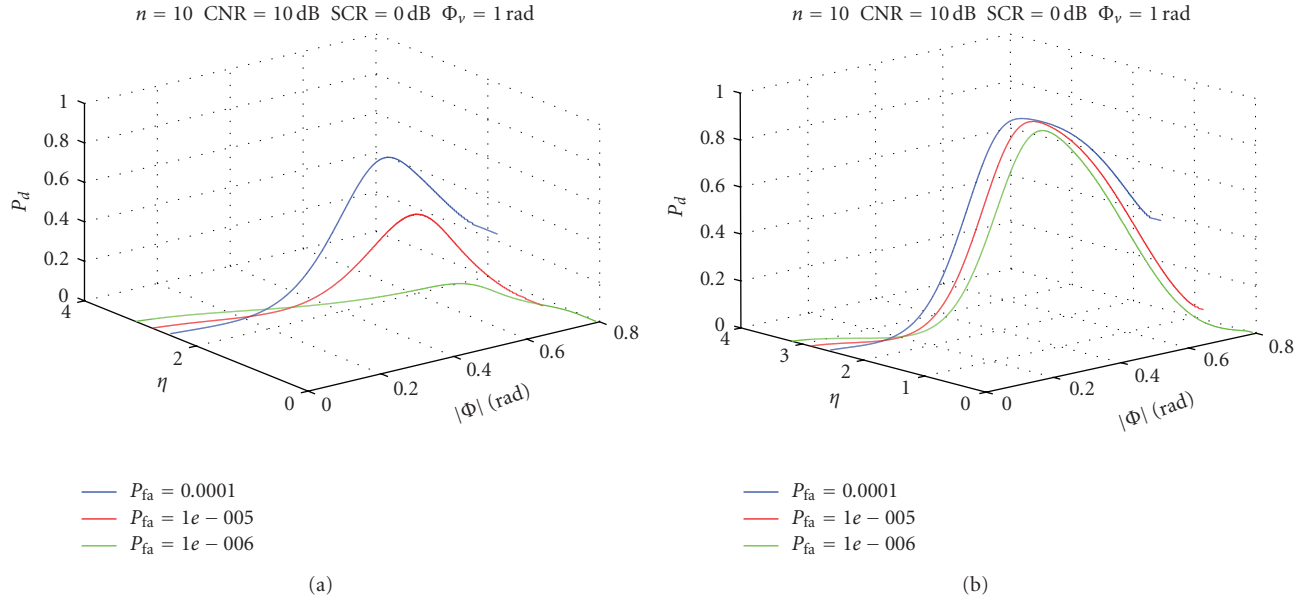
FIGURE 6: P_d curves along iso-P_{fa} curves with 3-D visualization for $P_{fa} = 1e - 4$, $1e - 5$, $1e - 6$, $n = 10$, CNR = 10 dB, SCR = 0 dB, and $\Phi_v = 1$ rad. (a) two-step CFAR detector with marginal PDFs; (b) Two-step CFAR detector with conditional PDF.

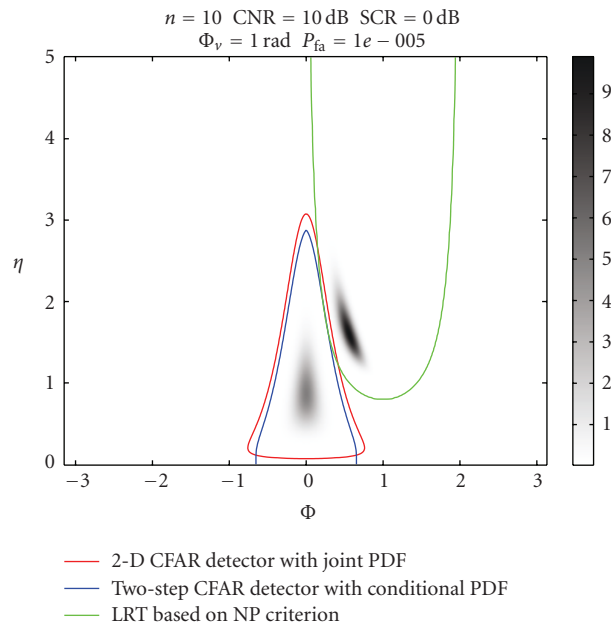FIGURE 7: Joint PDF of the two hypotheses and the threshold curves of ATI detectors for $n = 10$, CNR = 10 dB, SCR = 0 dB, $P_{fa} = 1e - 5$, $\Phi_v = 1$ rad. (two-step CFAR with conditional PDF, 2D CFAR with joint PDF, and LRT based on NP criterion).

test can be exploited to maximize the P_d with constant P_{fa} as follows,

$$\Lambda_{2D}(\eta, \Phi) = \frac{f(\eta, \Phi \mid H_1)}{f(\eta, \Phi \mid H_0)} = \frac{f_{c+m}(\eta, \Phi)}{f_c(\eta, \Phi)}$$

$$= \frac{C}{f_c(\eta, \Phi)} > \gamma, \quad \gamma > 0, \tag{10}$$

where C is a constant and γ is the detection threshold. Equation (10) can be simplified as constant-density contour lines on the magnitude-phase plane
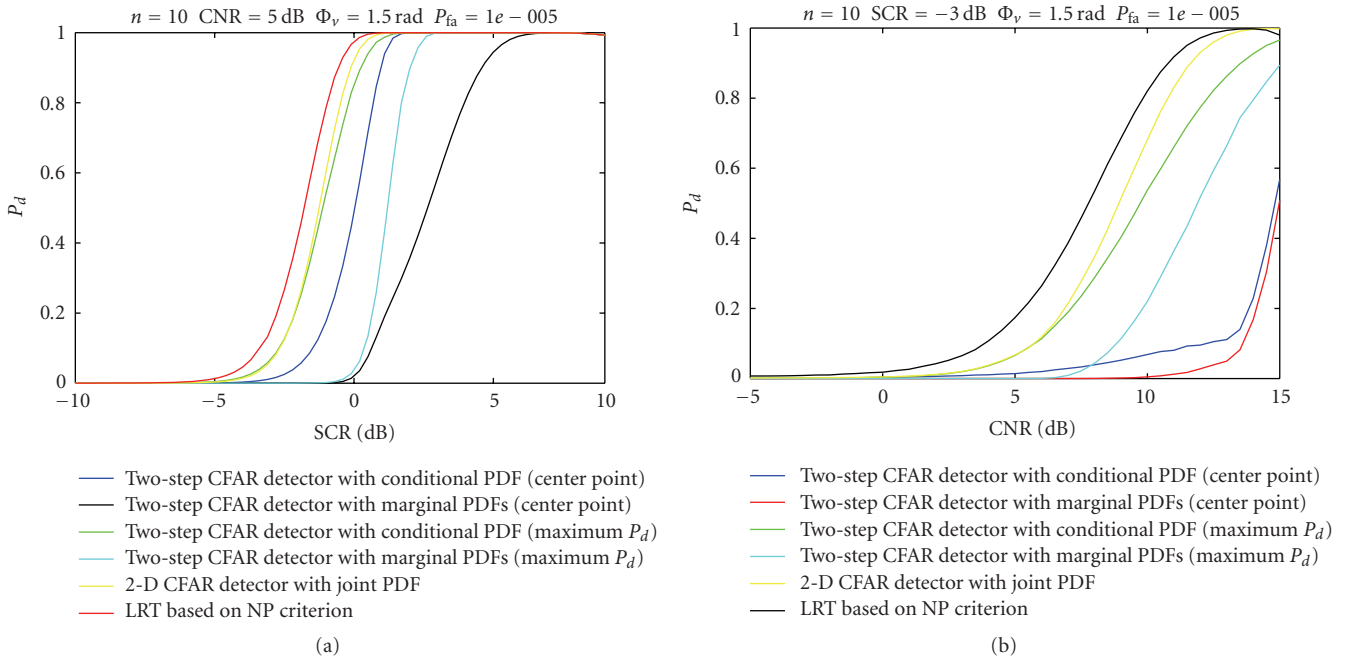
$$f_c(\eta, \Phi) < \gamma'. \tag{11}$$

FIGURE 8: P_d of ATI detectors versus SCR and CNR for $n = 10$, $P_{fa} = 1e - 5$, and $\Phi_v = 1.5$ rad, (two-step CFAR detector with conditional PDF (center point/maximum P_d), two-step CFAR detector with marginal PDFs (center point/maximum P_d), 2D CFAR detector with joint PDF, and LRT based on NP criterion). (a) CNR = 5 dB; (b) SCR = 0 dB.
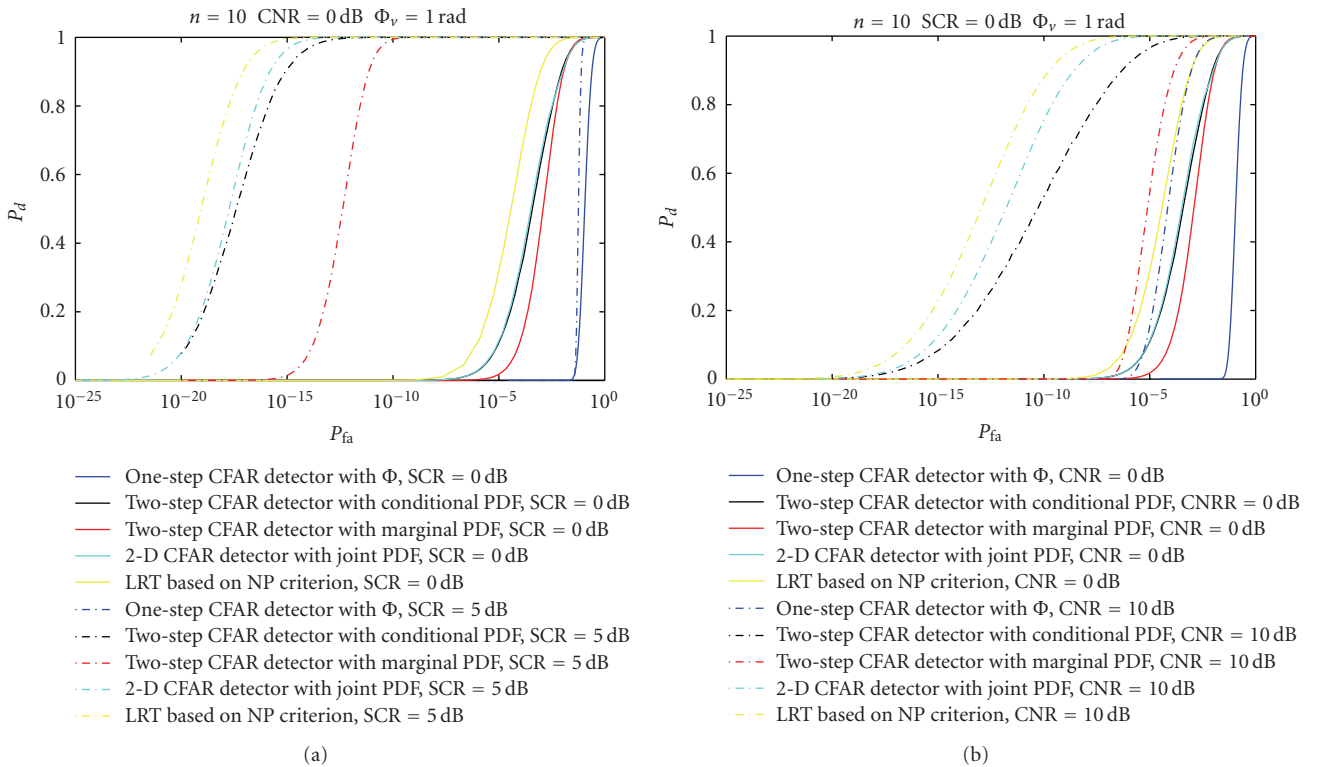

FIGURE 9: Performance of ATI detectors for SCRs and CNRs, $n = 10$, $\Phi_v = 1$ rad (one-step CFAR detector with, two-step CFAR detector with conditional PDF, two-step CFAR detector with marginal PDFs, 2D CFAR detector with joint PDF, and LRT based on NP criterion). (a) CNR = 0 dB, SCR = 0 dB, 5 dB; (b) SCR = 0 dB, CNR = 0 dB, 10 dB.
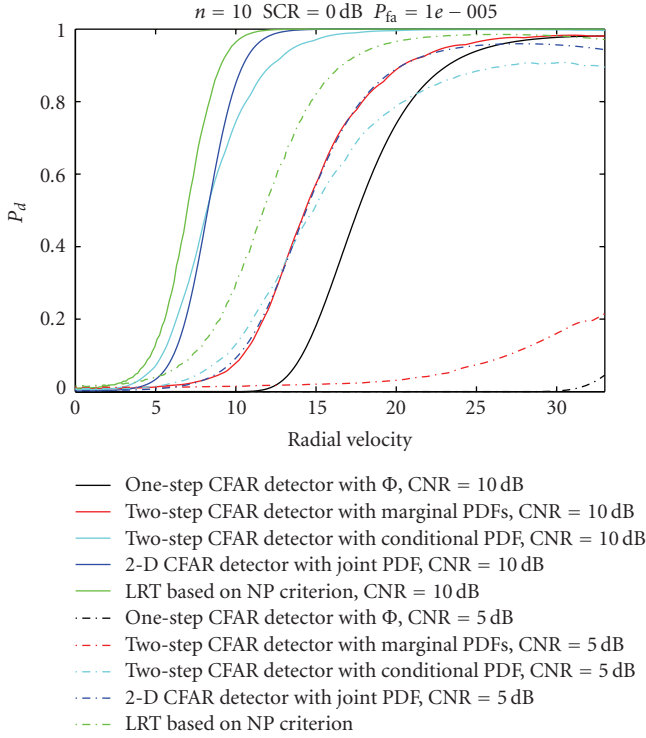
FIGURE 10: P_d of ATI detectors versus radial velocity of moving target for $n = 10$, $P_{fa} = 1e - 5$ (two-step CFAR detector with conditional PDF (center point/maximum P_d), two-step CFAR detector with marginal PDFs (center point/maximum P_d), 2D CFAR detector with joint PDF, and LRT based on NP criterion). SCR = 0 dB; CNR = 10, 5 dB.

The thresholds γ, γ' are determined by the P_{fa}:

$$
\begin{aligned}
P_{fa} &= \iint_{\Lambda_{2D}(\eta,\Phi)>\gamma} f_c(\eta,\Phi)\,d\eta\,d\Phi \\
&= \iint_{f_c(\eta,\Phi)<\gamma'} f_c(\eta,\Phi)\,d\eta\,d\Phi = \alpha.
\end{aligned}
\tag{12}
$$

P_d is simply the integral of the "Clutter plus moving target" PDF over the area where $f_c(\eta,\Phi) < \gamma'$. The above threshold curve is also plotted in Figure 7 with parameters given in Section 3.2.

3.4. The Likelihood Ratio Test Based on NP Criterion. In (4), the two target parameters Φ_v and δ (SCR) cannot be estimated directly from the interferometry data. However, because of the Doppler frequency shift between moving target and the clutter, the imaging results of the moving targets shift in the azimuth direction with respect to stationary scatter. Then, the target phase ψ caused by its cross-track motion can be expressed as

$$
\Phi_v = -\frac{\Delta a 2\pi B}{R_0 \lambda},
\tag{13}
$$

where Δa is the azimuth displacement, λ is the radar wavelength, B is the along-track baseline and R_0 is the

distance between the moving target and the satellite. In fact, except for some military applications of GMTI, a great deal of targets may travel strictly on the road or highway with specific moving direction and velocity range. Based on the road network database, such as road class, road location, road width and maximum velocity, the azimuth displacement map and the interferometric phase map of moving targets around the roads can be computed analytically pixel by pixel as stated in [4]. On the other hand, the RCS values of typical moving targets can also be derived from experimental measurement. These types of prediction may be interpreted as a priori knowledge that can be acquired, analyzed and integrated into the detection process of SAR-ATI for theoretical or engineering application [4]. Under a fixed P_{fa}, the likelihood ratio test function that maximizes the PD under the NP criterion is

$$
\Lambda(\eta,\Phi) = \frac{f(\eta,\Phi \mid H_1)}{f(\eta,\Phi \mid H_0)} = \frac{f_{c+m}(\eta,\Phi)}{f_c(\eta,\Phi)} > \mu, \quad \mu > 0.
\tag{14}
$$

The $f_{c+m}(\eta,\Phi)$, $f_c(\eta,\Phi)$ can be seen in (1) and (4). The corresponding parameters can be estimated with the method in [1] and the prior information. The iso-P_{fa} threshold curves can be determined by

$$
P_{fa} = \int_\mu^\infty f(\Lambda \mid H_0)\,d\Lambda = \int_{\{\eta,\Phi \mid \Lambda > \mu\}} f(\eta,\Phi \mid H_0)\,d\eta\,d\Phi = \alpha.
\tag{15}
$$

Simplification of the LRT function is a very difficult task and the numerical integration can be exploited to compute the P_{fa}, μ and P_d. Unfortunately, since the threshold curves for fixed P_{fa} depend on the signal parameters SCR and Φ_v, the LRT under the NP criterion does not possess the CFAR property.

Figure 7 plots the joint PDF of the two hypotheses, the threshold curves for two-step CFAR detection with conditional PDF, 2D CFAR detection with joint PDF, and LRT based on NP criterion. Figure 8 shows the P_d versus SCR and CNR with $n = 10$, $P_{fa} = 10^{-5}$, $\Phi_v = 1.5$ rad for two-step CFAR with conditional PDF (center point/maximum P_d), two-step CFAR with marginal PDFs (center point/maximum P_d), 2D CFAR with joint PDF, and LRT based on NP criterion. Figure 8 shows that the performance of two-step CFAR detector choosing the center point of the iso-P_{fa} curves is much poorer than the two-step CFAR detector using the threshold for maximum P_d. Moreover, the performance of the two-step CFAR detector using the threshold for maximum P_d is much close to the 2D CFAR detector with joint PDF.

4. Performance Analysis and Comparisons

4.1. Receiver Operating Characteristics. To measure the quality of the ATI CFAR detectors, Receiver Operating Characteristics (ROC) curves for different SCRs and CNRs are exploited, that is, P_d versus P_{fa} for different parameters. Figure 9 shows ROC curves versus SCR and CNR with $n = 10$, $\Phi_v = 1$ rad, and $P_{fa} = 10^{-5}$ for one-step CFAR

detector with Φ, two-step CFAR with conditional PDF, two-step CFAR with marginal PDFs, 2D CFAR detector with joint PDF and LRT based on NP criterion, CNR = 0 dB, SCR = 0 dB, 5 dB; and SCR = 0 dB, CNR = 0 dB, 10 dB. To compare the performance much clearly, the axis of P_{fa} is used as log-coordinate. The performance of one-step CFAR detector with Φ is much poorer than other detectors. The LRT based on NP criterion yields a benchmark performance for other detectors. Under some SCRs or CNRs, the two-step CFAR detector with conditional PDF shows much better performance than the 2D CFAR detector. The performance of the two-step CFAR detector is much worse than the other $\eta - \Phi$ detectors, especially under low SCR condition.

4.2. Probability of Detection versus Radial Velocities of Moving Target. Another measure of the ATI CFAR detectors' quality is P_d versus the radial velocities of moving target for different SCRs and CNRs. Figure 10 shows P_d versus the radial velocity with $n = 10$, $V_r = 0 : 35$ m/s, and $P_{\text{fa}} = 10^{-5}$ for one-step CFAR detector with Φ, two-step CFAR with conditional PDF, two-step CFAR with marginal PDFs, 2D CFAR detector with joint PDF and LRT based on NP criterion, for SCR = 0 dB, CNR = 0 dB, 10 dB. The radar system parameters are: satellite speed $V_s = 7.6$ Km/s, altitude $H = 625.87$ Km, center frequency 9.65 GHz, PRF = 3.15 KHz, along-track baseline 2.4 m, antenna size (length × width) 5.4 m × 0.9 m, chirp bandwidth CB = 100 MHz. The minimum detectable velocity (MDV) as an important system design parameter is limited by the radar parameters, P_{fa}, P_d, target RCSs, and signal processing and detection techniques. Based on the above parameters, P_d is 0.9. Figure 10 shows that the two-step CFAR detector with conditional PDF and the 2D CFAR detector with joint PDF may improve the MDV significantly. The one-step CFAR detector with Φ shows much poorer performance than the other detectors, which only obtain very low P_d under low SCR or CNR conditions. The analysis results provide a way to spaceborne SAR-ATI systems quality measure and system design.

5. Conclusion

In this paper, based on the theoretical PDF of interferogram's amplitude-phase for the two hypotheses, several ATI CFAR detectors are analyzed under low SCR or low CNR conditions. The LRT based on the NP criterion yields an upper bound performance for the other detectors. The 2D CFAR detector shows a close performance to the optimum LRT detector, which is also ease to be applied to process the real data. In [1], the author also proposed the theoretical joint PDF for the heterogeneous clutter and the extremely heterogeneous clutter regions. The CFAR detectors analyzed in the paper can also be used under these conditions.

Acknowledgments

References

[1] C. H. Gierull, "Statistical analysis of multilook SAR interferograms for CFAR detection of ground moving targets," *IEEE Transactions on Geoscience and Remote Sensing*, vol. 42, no. 4, pp. 691–701, 2004.

[2] C. H. Gierull, "Moving target detection with along-track SAR interferometry: a theoretical analysis," Tech. Rep. DRDC-OTTAWA-TR-2002-084, Defence Research and Development, Ottawa, Canada, August 2002.

[3] S. Chiu, "A constant false alarm rate (CFAR) detector for RADARSAT-2 along-track interferometry," *Canadian Journal of Remote Sensing*, vol. 31, no. 1, pp. 73–84, 2005.

[4] F. Meyer, S. Hinz, A. Laika, D. Weihing, and R. Bamler, "Performance analysis of the TerraSAR-X traffic monitoring concept," *ISPRS Journal of Photogrammetry & Remote Sensing*, vol. 61, no. 3-4, pp. 225–242, 2006.

[5] S. Chiu, "Clutter effects on ground moving target velocity estimation with SAR along-track interferometry," in *Proceedings of International Geoscience and Remote Sensing Symposium (IGARSS '03)*, vol. 2, pp. 1314–1319, Toulouse, France, July 2003.

[6] S. Chiu and C. Livingstone, "A comparison of displaced phase centre antenna and along-track interferometry techniques for RADARSAT-2 ground moving target indication," *Canadian Journal of Remote Sensing*, vol. 31, no. 1, pp. 37–51, 2005.